Photoionized plasmas induced in neon with extreme ultraviolet and soft X-ray pulses produced using low and high energy laser systems

A. Bartnik, P. Wachulak, T. Fok, Ł. Węgrzyński, H. Fiedorowicz, T. Pisarczyk, T. Chodukowski, Z. Kalinowska, R. Dudzak, J. Dostal, E. Krousky, J. Skala, J. Ullschmied, J. Hrebicek, and T. Medrik

Citation: Physics of Plasmas **22**, 043302 (2015); doi: 10.1063/1.4919024
View online: http://dx.doi.org/10.1063/1.4919024
View Table of Contents: http://scitation.aip.org/content/aip/journal/pop/22/4?ver=pdfcov
Published by the AIP Publishing

Photoionized plasmas induced in neon with extreme ultraviolet and soft X-ray pulses produced using low and high energy laser systems

A. Bartnik,[1] P. Wachulak,[1] T. Fok,[1] Ł. Węgrzyński,[1] H. Fiedorowicz,[1] T. Pisarczyk,[2] T. Chodukowski,[2] Z. Kalinowska,[2] R. Dudzak,[3] J. Dostal,[3] E. Krousky,[3] J. Skala,[3] J. Ullschmied,[3] J. Hrebicek,[3] and T. Medrik[3]
[1]*Institute of Optoelectronics, Military University of Technology, Kaliskiego 2, 00-908 Warsaw, Poland*
[2]*Institute of Plasma Physics and Laser Microfusion, 23 Hery St., 00-908 Warsaw, Poland*
[3]*Institute of Plasma Physics ASCR, Prague, Czech Republic and Institute of Physics ASCR, Prague, Czech Republic*

(Received 18 February 2015; accepted 13 April 2015; published online 24 April 2015)

A comparative study of photoionized plasmas created by two soft X-ray and extreme ultraviolet (SXR/EUV) laser plasma sources with different parameters is presented. The two sources are based on double-stream Xe/He gas-puff targets irradiated with high (500 J/0.3 ns) and low energy (10 J/1 ns) laser pulses. In both cases, the SXR/EUV beam irradiated the gas stream, injected into a vacuum chamber synchronously with the radiation pulse. Irradiation of gases resulted in formation of photoionized plasmas emitting radiation in the SXR/EUV range. The measured Ne plasma radiation spectra are dominated by emission lines corresponding to radiative transitions in singly charged ions. A significant difference concerns origin of the lines: K-shell or L-shell emissions occur in case of the high and low energy irradiating system, respectively. In high energy system, the electron density measurements were also performed by laser interferometry, employing a femtosecond laser system. A maximum electron density for Ne plasma reached the value of $2{\cdot}10^{18}\,\mathrm{cm}^{-3}$. For the low energy system, a detection limit was too high for the interferometric measurements, thus only an upper estimation for electron density could be made. © *2015 AIP Publishing LLC*. [http://dx.doi.org/10.1063/1.4919024]

I. INTRODUCTION

Photoionized plasmas (PP) can be produced by irradiation of gases with X-ray or extreme ultraviolet (EUV) photons. These plasmas are not present in normal conditions on Earth but are common in Space, where X-ray or EUV radiation is emitted by different astrophysical objects. Such radiation can propagate for long distances and ionize the interstellar media or planetary atmospheres. In laboratory conditions, these kinds of plasmas can be created in a vacuum environment by irradiation of either gases[1,2] or low temperature laser-produced plasmas (LPP)[3] with high energy photons. In contrary to ionization processes encountered in LPP which are induced with low energy photons, photoionization mechanism does not require overcoming of any intensity threshold. It does not mean, however, that photoionized plasmas can be produced by a radiation field with arbitrarily small intensity, due to finite time of recombination processes and necessity to fulfill criteria for plasmas. Nevertheless, intensity of the ionizing radiation for photoionized plasma creation can be orders of magnitude lower comparing to LPP.

Photoionization of gases is one of the most important process in the formation of different kinds of astrophysical plasmas, especially located close to strongly radiating compact objects. The information about the parameters of these plasmas is obtained mainly from spectral measurements. The interpretation of the observed spectra is based on computer modelling and laboratory experiments that support the accuracy of the physical models. A number of attempts for laboratory simulation of such plasmas employing high intensity X-ray sources with spectral distribution close to blackbody radiation have been performed. X-ray radiation, necessary for such experiments, can be created in high temperature plasmas of high electron density. The creation of such plasmas required high power discharge or laser systems called high-energy density (HED) facilities. Some laboratory experiments concerning astrophysical photoionized plasmas were performed using the GEKKO XII (Ref. 3) and Shenguang II (Ref. 4) high-power laser facilities and the Z pulsed-power facility.[1,2] In these experiments, the irradiated media were located close to the X-ray radiating plasmas. The energy flux of X-ray radiation in the extreme cases exceeded $10^{11}\,\mathrm{W/cm}^2$ and was sufficient for the formation of photoionized plasma with high ionization degree. A brief review of interpretation of astrophysical observations, supported by the laboratory astrophysics experiments, was presented previously.[5]

Some of photoionized plasmas present in Space are not driven by strongly X-ray radiating objects. The plasmas induced in upper planetary atmospheres could be taken as example. Photoionization of atoms and molecules is one of the dominant process that occurs in these regions.[6–10] The laboratory simulation of plasmas induced in such conditions does not require extremely high X-ray radiation field. Evidently, the significant part of solar electromagnetic radiation is emitted in the EUV range. In addition to that the energies of the EUV photons are comparable to the binding energies of valence electrons and the energies required for dissociative photoionization. As a result, the cross sections for processes induced by the EUV photons are much higher comparing to

the X-ray photons.[11–14] In this case, photoionized plasmas can be created using EUV pulses of moderate intensity, accessible from compact laboratory-scale sources. The corresponding experiments were performed using LPP sources at radiation intensity of the order of 10^7–10^9 W/cm^2.[15–19]

In this work, photoionized plasmas were created by irradiation of gases with intense EUV and soft X-ray (SXR) pulses. The EUV/SXR pulses were produced by two different laser produced plasma sources with significantly different parameters. The differences concerned the photon energy range and the radiation power density. The SXR/EUV beam was focused using grazing incidence focusing mirrors onto the gas stream that was injected into the beam-gas interaction region. The injection of the gas was synchronous with the radiation pulse. The emission spectra of the photoionized plasmas were recorded and comparative investigations were performed. The electron density measurements were performed by employing the laser interferometry method. The interferograms were acquired by using a femtosecond laser system. The density distributions were obtained from the recorded interferograms. The spectral measurements performed in the SXR/EUV range allowed to obtain emission spectra corresponding to K- and L-shell emission from single and multiple charged Ne ions. Significant differences in emission spectra and electron densities between photoionized plasmas created using different irradiation parameters were observed.

II. EXPERIMENTAL ARRANGEMENTS

Two different laser systems were employed for the production of the EUV/SXR pulses, used for the creation of photoionized plasmas. The first one was a Nd:YAG laser system with a SBS (Stimulated Brillouin Scattering) mirror giving 10 J/1 ns pulses with 10 Hz repetition rate (NL 129 from EKSPLA, Lithuania), working at the fundamental wavelength 1.06 μm. The second one was the kJ-class iodine laser system located at the PALS Research Centre, Prague, Czech Republic. The PALS laser system produced single pulses with time duration of 350 ps at the fundamental wavelength 1.315 μm. For both systems, the laser pulse was focused onto a double stream gas puff target, created synchronously with the laser pulse. The gas puff target was created by pulsed injection of xenon into a hollow stream of helium (Xe/He gas puff target), by using electromagnetic valve system. The valve system was equipped with a double nozzle set-up. The detailed description of the double stream gas puff target can be found elsewhere.[20,21]

In Fig. 1, an experimental arrangement based on the NL 129 laser system is presented. The LPP being a point-like source of intense EUV/SXR radiation was created in the focal point of a grazing incidence paraboloidal mirror. A quasi-parallel radiation beam, formed this way, was focused using the second, identical mirror onto another gas stream injected synchronously with the EUV/SXR pulse into the interaction region. The irradiation of the injected gas with the ionizing radiation from the LPP source resulted in a photoionized plasma formation. The EUV emission spectra from the photoionized plasma were measured using a home-made

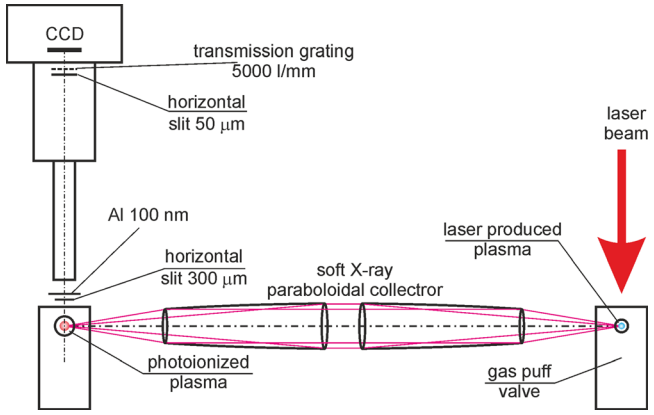

FIG. 1. Schematic view of the experimental arrangement for photoionized plasma creation employing the NL 129 Nd:YAG laser system.

spectrograph, consisted of a 5000 l/mm transmission grating, a back-illuminated CCD camera, DX420-BN Andor and a 50 μm wide entrance slit (TG spectrograph). The grating is 0.5 μm-thick, 4×10 mm^2 in size, free-standing gold grating with the support mesh consisting of a 4 μm-period grating crossed with a 150 μm-period grating.[22] Due to low intensity of the expected emission from the photoionized plasma, it was necessary to place the CCD detector as close to the plasma as possible. To assure a necessary spectral resolution of at least $\lambda/\Delta\lambda \approx 50$ for the interesting wavelength range (30–70 nm) an auxiliary 300 μm wide slit was placed between the entrance slit of the spectrograph and the photoionized plasma. The distance between the auxiliary slit and plasma was about 20 mm. To reduce the CCD background, originating from the visible light, the radiation was filtered using a 100 nm thick aluminum foil.

The basic experimental arrangement using the PALS laser system is demonstrated in Fig. 2. In this case, the gas to be ionized was injected in the vicinity of the laser plasma at a distance of approximately 15 mm. The injected gas was directly irradiated without the use of focusing collector. The gas stream was injected by an elongated nozzle, in the form

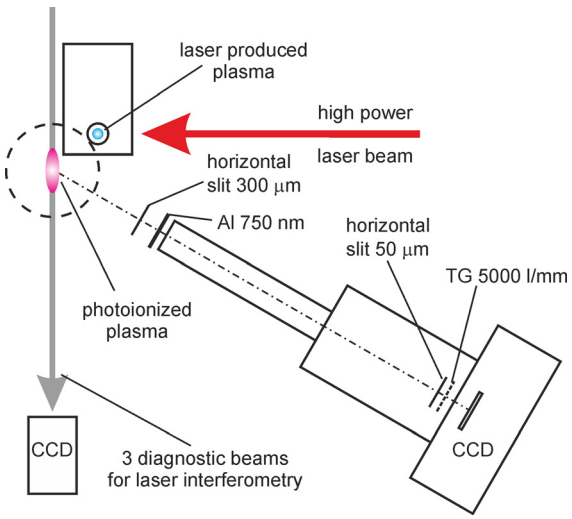

FIG. 2. Schematic view of the basic experimental arrangement for photoionized plasma creation by the direct irradiation of the gas injected in the vicinity of the laser plasma, employing the PALS iodine laser system.

of $0.5 \times 9\,\text{mm}^2$ slit, located off axis, perpendicularly to the laser beam.

To measure the spatial and temporal changes in the electron density of the photoionized plasma, a three-frame interferometric system[23] irradiated by the Ti:Sa femtosecond laser (pulse duration ~ 40 fs/wavelength 0.8 μm) was used.[24] Each channel of the interferometer was equipped with a CCD camera (RM-4200 GigEV), enabling registration of the interferograms with high spatial resolution (2048×2048 pixels with a size of $\sim 6 \times 6\ \mu\text{m}^2$) and 16-bit dynamic range. Three-frame sequences of the interferograms with preselected delay between the frames were recorded. The delay for the first frame is measured with respect to the maximum intensity of the main laser pulse.

The SXR/EUV emission spectra from the photoionized plasma were measured using the TG spectrograph. In this case, however, the ultra-thin 100 nm Al foil used in the previous setup was replaced by a 750 nm thick foil, as the strong shock was destroying the ultra-thin foil in a single shot.

Figure 3 demonstrated the optional experimental arrangement employing the PALS laser system. In this case the laser plasma radiation was focused using the paraboloidal collector onto the gas stream injected synchronously with the SXR pulse into the interaction region. In this configuration, only spectral measurements for photoionized plasmas were performed. The optical axis of the TG spectrograph was oriented perpendicularly to the optical axis of the collector Therefore, the emission spectra from the photoionized plasmas were not affected by the laser plasma emission. The gas puff nozzle produced debris due to interaction with high temperature laser plasma. To protect the SXR collector from the nozzle debris two 750 nm thick Al foils were placed in front of the collector. These foils worked additionally as the SXR filter with approximately 80% transmission at $\lambda = 1$ nm wavelength. Unfortunately despite the protection foils after several pulses the collector surface was significantly degraded, hence, most of the experimental results were obtained using the basic experimental arrangement.

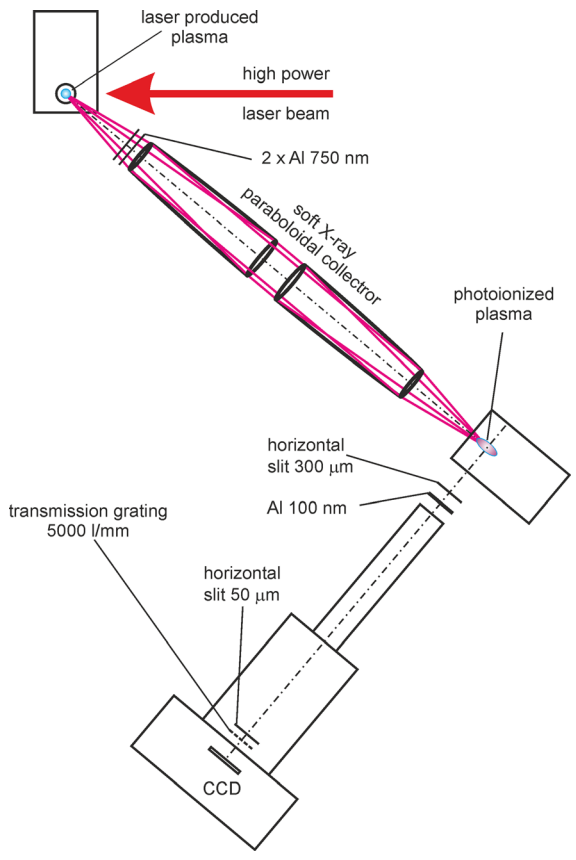

FIG. 3. Schematic view of the optional experimental arrangement for photoionized plasma creation, employing the PALS iodine laser system.

In Fig. 4, SXR emission spectra for laser plasmas produced using both laser systems are presented. The spectra were measured using the TG spectrograph, however, in this case, the diffraction grating and the CCD detector were placed at longer distances. This enabled better spectral resolution of $\lambda/\Delta\lambda \approx 100$ at 10 nm wavelength. In both cases, strong peaks at the wavelength close to 1 nm were observed. Significant difference concerned radiation emission at longer wavelengths. In case of the experimental arrangement using the NL 129 laser system (Fig. 4(a)) intense emission spans the wide wavelength range, with wide-band spectral maxima around 5 and 11 nm. In case of the spectrum obtained using the PALS laser system (Fig. 4(b)), spectral intensity beyond 2 nm decreases more or less monotonically. However, spectrally integrated intensities in both ranges (below and above 2 nm wavelength) were comparable.

The energy fluence for the focused SXR/EUV radiation, produced using the NL 129 laser system, was measured using a calibrated pinhole coupled to the AXUV 100 detector. The pinhole with 10 μm diameter was mounted on an XY translation stage and placed in the focal plane of the collector, close to its axis. The AXUV detector was reversely polarized with the voltage 30 V and placed downstream the pinhole, at distance allowing the registration of the entire radiation passing through the pinhole. Position of the pinhole was adjusted such as to obtain the maximum of the detected signal. The radiation fluence calculated for the maximum value of the signal reached 0.2 Jcm^{-2}.

In case of the experimental arrangement using the PALS laser system for laser plasma creation (Fig. 2), the photoionized plasmas were created by direct SXR irradiation without using any collector. In this case, the fluence was measured without any pinhole, using a silicon detector BPYP 03 located at a distance of approximately 2.5 m from the laser plasma. To avoid visible light reflected from the walls of the

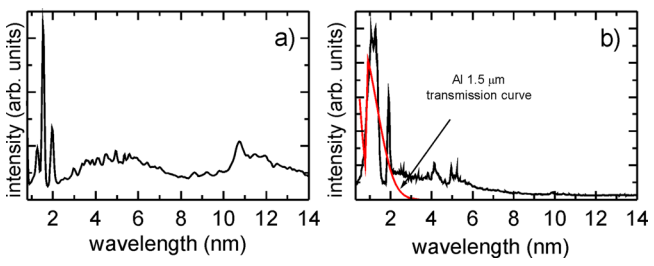

FIG. 4. Emission spectra for laser plasmas produced by irradiation of Xe/He gas puff targets with laser pulses from: (a) NL 129 and (b) PALS laser systems.

vacuum chamber and metal tubes a 15 μm thick beryllium filter was mounted in front of the detector. Based on the detected signal and assuming $1/r^2$ dependence of the radiation intensity, the SXR fluence at a distance of 15 mm from the laser plasma, where the gas for photoionization was injected, was estimated to be 2 Jcm^{-2} for the laser pulse energy of 500 J.

III. EXPERIMENTAL RESULTS

Photoionized plasmas were created in different atomic and molecular gases. The time integrated optical images of photoionized plasmas, produced using the SXR/EUV irradiation system based on the NL 129 Nd:YAG laser, are presented in Fig. 5. In case of plasmas created in atomic gases (Figs. 5(a)–5(c)), intense emission areas close to the optical axis of the SXR collector were visible. Lateral size of the emission regions corresponds to a cross section of the SXR/EUV beam. Additionally, in case of neon (Fig. 5(a)), the visible light was emitted from a large low-density area surrounding the interaction region. The intensity of the optical emission from plasmas created in SF_6 gas (Fig. 5(d)), was a few times lower comparing to the other gases and the emission originates only from the near-axis region. The images were obtained for the photoionized plasmas created in gases injected into the interaction region with relatively low density, $n \approx 10^{17}\,cm^{-3}$. An increase in the density resulted in formation of the photoionized plasma upstream the focal point of the irradiating beam.

The spectral measurements performed in a wide SXR/EUV wavelength range allowed to obtain a spectrum only for Ne plasma. In case of other gases only the 0th order was detected. Although for the photoionized plasma induced in SF_6 even the 0th order was hardly visible. A single Ne spectrum was quite weak. Therefore to obtain a good signal-to-noise ratio, it was integrated over 25 pulses. The spectrum consisted of multiple lines in the EUV range, originating mainly from the transitions in singly charged ions (Ne II). However also contained well pronounced spectral lines, corresponding to $2s^22p^6$–$2s^22p^53s$ and $2s^22p^4$–$2s2p^5$ transitions

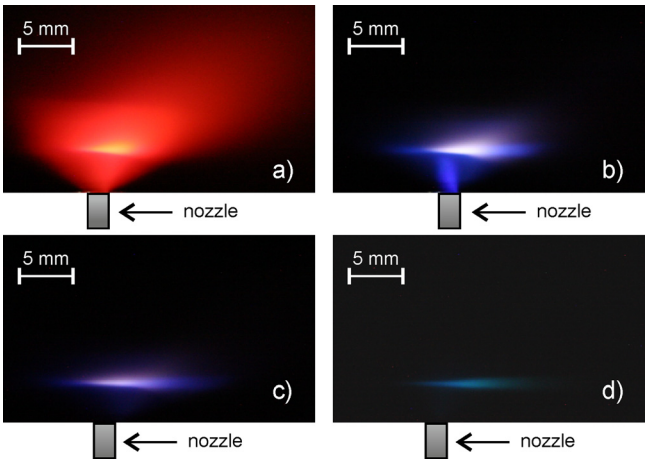

FIG. 5. Optical images of photoionized plasmas created in atomic and molecular gases using the NL 129 Nd:YAG laser system: (a) Ne, (b) Kr, (c) Ar, (d) SF_6. Position of the nozzle for the gas injection was shown.

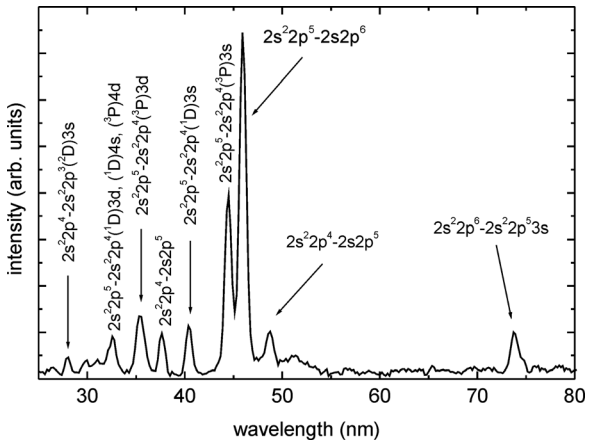

FIG. 6. Emission spectrum obtained from photoionized plasma created in Ne gas using the NL 129 Nd:YAG laser system. The spectrum was integrated over 25 pulses.

in Ne I and Ne III species, respectively. No spectral lines were detected in the short wavelength range ($\lambda < 28$ nm). The spectrum is presented in Fig. 6.

In addition to the spectral measurements, attempts to measure electron density of the photoionized plasma by laser interferometry, using a part of the main laser beam of the Nd:YAG system, were carried out. The measurements were performed for both fundamental and second harmonic of the laser beam, for different gases and injection parameters. However, the interference patterns in all cases acquired for photoionized plasmas exhibited no fringe shift with respect to neutral gases. This means that the differences in optical paths were below the detection limit.

Significantly different results were obtained for experimental conditions using the high power laser PALS. In Fig. 7, emission spectra labelled as S1 and S2, obtained for Ne photoionized plasmas employing experimental arrangements shown in Figs. 2 and 3, respectively, are presented. Both spectra contain strong emission peaks, corresponding to Ne II K_α line that were not detected in case of using the experimental arrangement based on the Nd:YAG laser. A

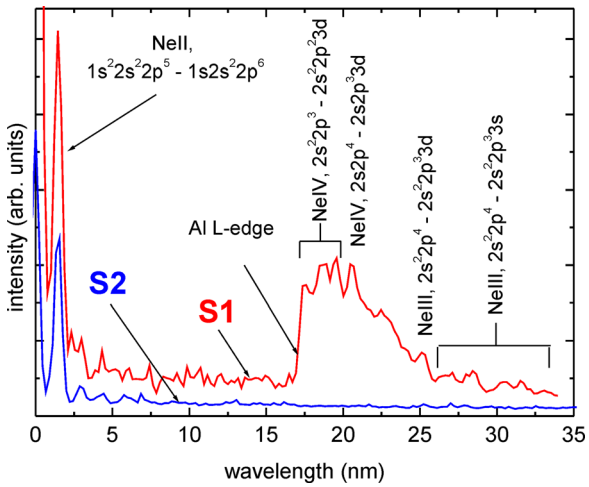

FIG. 7. Emission spectra obtained from photoionized plasma created in Ne gas using the PALS laser system. S1, S2—spectra obtained using the experimental arrangements, shown in Figs. 2 and 3, respectively.

significant difference between the spectra concerns the long wavelength region. The S1 spectrum except the K_α line contains a series of overlapping lines in the wavelength range of 17–35 nm. The lines were identified as corresponding to $2s^22p^3$–$2s^22p^23d$, $2s2p^4$–$2s2p^33d$ transitions in Ne IV ions and $2s^22p^4$–$2s^22p^33d$, $2s^22p^4$–$2s^22p^33s$ in Ne III ions. The lines that would be emitted with the wavelengths shorter than 17 nm were unfortunately absorbed by the Al filter. The S2 spectrum contains exclusively Ne II K_α line with the intensity approximately two times lower comparing to the S1 spectrum.

The interferometric investigations were performed either for laser plasmas or photoionized plasmas. As explained earlier, the registration time of frames referred to the maximum intensity of the main laser pulse, creating the laser plasma. In Fig. 8, a temporal sequence of interferograms obtained for Xe laser plasmas is presented. Due to strong opacity of Xe plasmas for the diagnostic radiation, it was not possible to calculate the electron density. Nevertheless, it can be noticed that the laser plasma formation starts over 0.8 ns before the arrival of the maximum of the laser pulse (t = 0) and it was being formed within approximately 1 ns. At a time 0.8 ns after the laser pulse maximum the Xe plasma is well formed and its shape is maintained for another 1 ns.

The results of the interferometric measurements of the photoionized plasmas, created using the experimental arrangement shown in Fig. 2, allowed to calculate the electron densities for plasmas created in neon and other gases. The photoionized plasma geometry is not axially symmetric, due to the shape of the gas-puff nozzle. Therefore, the electron density distributions cannot be calculated using the Abel transformation. For this reason, the average electron density distributions in the photionized plasma stream with the length corresponding to the longitudinal dimension of the gas-puff nozzle ($l_p = 0.9$ cm) had been calculated. The calculations were performed with the use of relations between the phase and electron density in fully ionized plasma[25]

$$\delta(y, z) = 4.46 \cdot 10^{-14} \lambda \bar{n}_e(y, z) l_p, \tag{1}$$

where δ (y, z)—phase increase of the probing beam with wavelength λ, along the plasma having the length l_p The average electron density distribution ($\bar{n}_e$) was defined as

$$\bar{n}_e(y, z) = \frac{\int_0^{l_p} n_e(x, y, z)dx}{l_p}. \tag{2}$$

Based on the information about the average electron density distributions, the linear density (N_e), and consequently the total electron number (N) in the stream of the photoionized plasma have been determined.

In case of Ne plasmas, two sets of good quality interferograms were acquired within the time duration of the laser plasma. In both cases, the first interferograms were acquired before the arrival of the laser pulse maximum, at t = −409 ps and t = −187 ps, respectively. In both cases, no fringe shift with respect to the neutral gas was detected. A pronounced fringe shift was detected in both cases for interferograms recorded 1 and 2 ns later on. In Fig. 9, the electron density distributions calculated for interferograms acquired for t = 591 ps and t = 1591 ps are presented. In both cases, maximum of the electron density, located close to the outlet of the nozzle, had more or less the same value of approximately $2 \cdot 10^{18}$ cm^{-3}. The electron densities integrated over planes perpendicular to the axis of the gas flow and total electron densities had higher values for t = 1591 ps time.

Unfortunately, no interferogram for Ne plasma was obtained for t ≈ 0, hence no information about the photoionized Ne plasma formation for this time was available. On the other hand, interferograms for other gases like Ar, Kr or Xe, at t = −34 ps, +19 ps and +33 ps were acquired, respectively. However, in the case of Ar the fringe shift was hardly detectable, interference patterns obtained for Kr and Xe indicate the plasma existence. In Fig. 10, electron density distribution for Xe plasma, formed at t = 33 ps, is presented. The maximum electron density in this case was approximately two times lower comparing to the density calculated for Ne plasma at t = 591 ps.

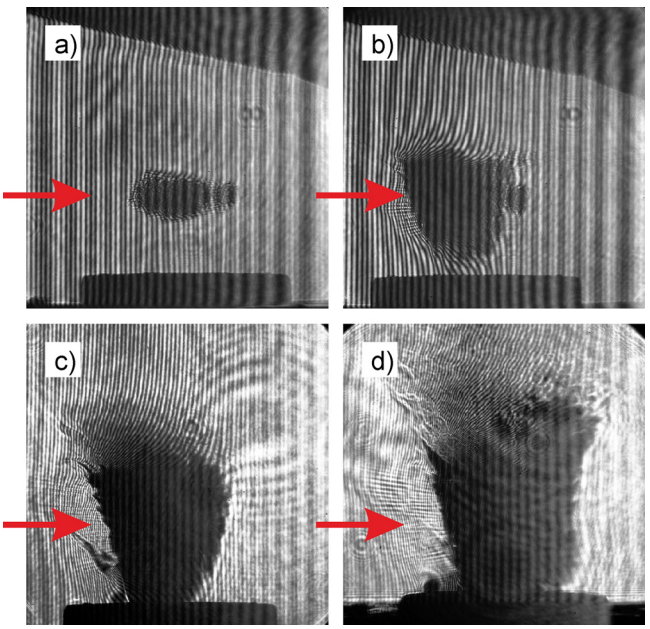

FIG. 8. Interferograms of the laser plasmas, acquired for different delays with respect to the laser pulse maximum at t = 0: (a) t = − 824 ps, (b) t = − 364 ps, (c) t = −145 ps, (d) t = 855 ps. Arrows indicate the incident laser beam direction and vertical position with respect to the nozzle outlet.

IV. DISCUSSION OF THE RESULTS

Formation of photoionized plasmas differs significantly from the formation of the laser produced plasmas. In the latter case, the energy of a single photon remains far below an ionization threshold of atoms particularly, of the multiply charged ions. In this case, free electrons are accelerated in a strong optical field gaining sufficiently high energy for the ionization or the excitation of atoms or ions. The acceleration is a continuous process during which outer electrons are released and consecutive ionization stages are achieved. In case of photoionized plasmas, driven by EUV or SXR radiation, the situation is significantly different. A single EUV/SXR photon is capable for ionization or excitation of atoms

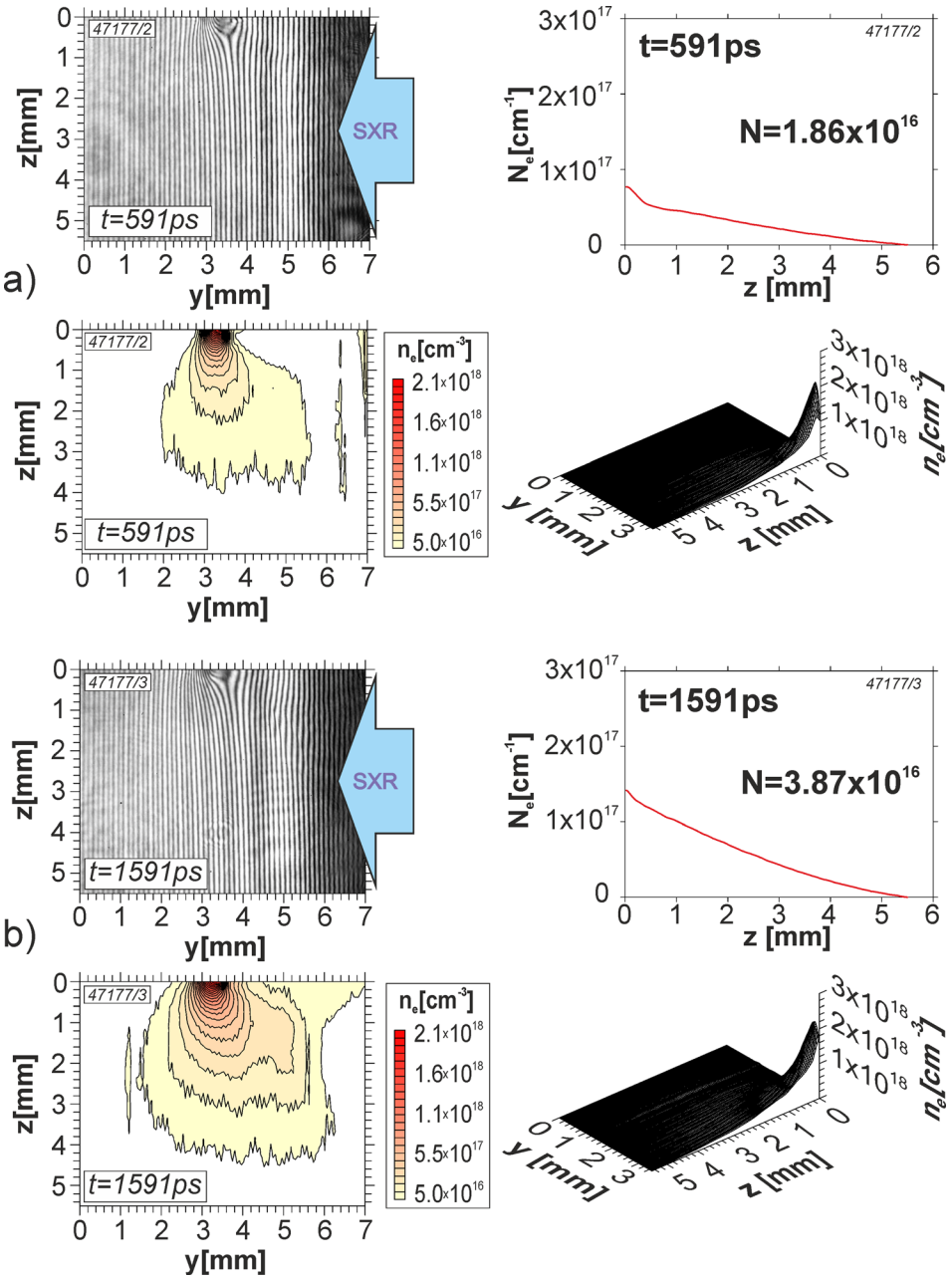

FIG. 9. Electron density distributions for Ne photoionized plasmas, obtained using the experimental arrangement shown in Fig. 2, acquired for two delay times with respect to the arrival of the laser pulse maximum: (a) t = 591 ps, (b) t = 1591 ps.

or ions. The energy of the resulting photoelectron usually remains sufficiently high for further ionization or excitation. In addition to that the inner shell ionization cannot only be followed by radiative decay but also by autoionization. This can turned into a dominating process. The electrons released in this process as well as photoelectrons lose their energies in a few collisions and practically do not gain energy from the radiation field. The electron temperature remains thus low, with significant contribution of energetic non-thermal electrons.

Significant differences between spectra shown in Figs. 6 and 7 are mainly associated with different energies of the driving photons. The first spectrum was obtained for photoionized plasmas formed in Ne gas irradiated with EUV/SXR photons having the spectrum shown in Fig. 4(a). In this case, only a few percent of the driving photons have energies exceeding the binding energy of K-shell electrons in Ne atoms. Beside that the total fluence of the driving radiation is one order of magnitude lower compared to the SXR radiation emitted from the plasmas produced by the PALS laser pulses. In this case, the Ne K_α photons were not detected. On the other hand photons from the wavelength range $\lambda < 25.5$ nm have energies exceeding the binding energy of the electrons localized in the $2s^2$ Ne subshell. The electron release from this subshell results in an excited $1s^2 2s 2p^6$ state of the Ne II ion. This state cannot decay through autoionization, as its deexcitation energy $E \approx 26.8$ eV is far below the ionization energy of Ne II ion ($E \approx 40.9$ eV). In addition to that the electron impact deexcitation rate is negligible due to low density of electrons and the excited ions. In this case, the radiative transition $2s^2 2p^5 – 2s 2p^6$ is the most probable decay channel, resulting in an intense spectral line at $\lambda = 46.1$ nm. It should be noted that the creation of the $1s^2 2s 2p^6$ excited state via ionization from the ground state of neutral atoms is a single event process. Other excitations of Ne II ions must be preceded by ionization of the neutral

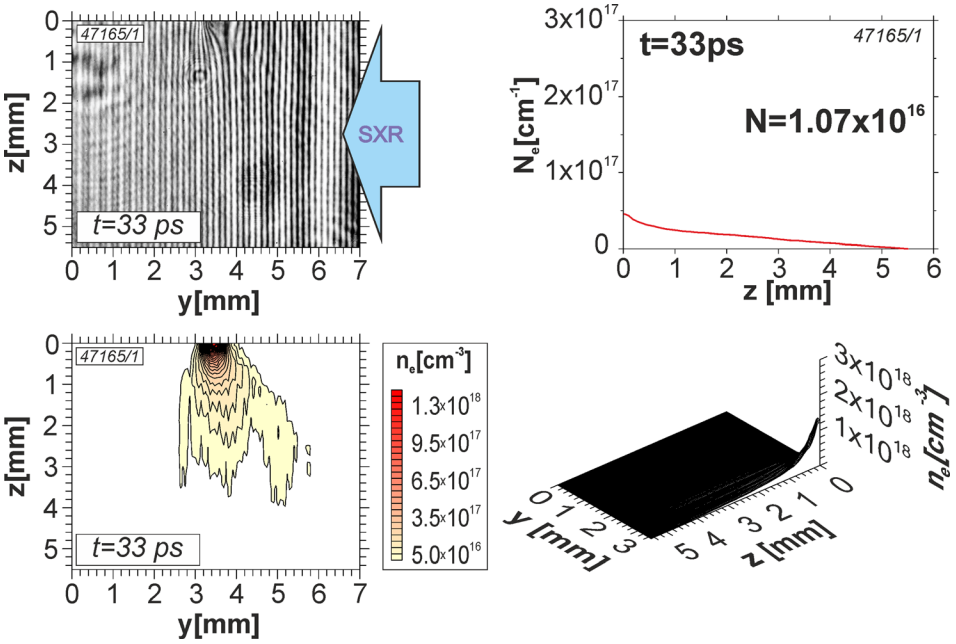

FIG. 10. Electron density distributions for Xe photoionized plasma, obtained using the experimental arrangement shown in Fig. 2, acquired for t = 33 ps delay time with respect to the arrival of the laser pulse maximum.

atoms. Therefore, the line corresponding to the $2s^2 2p^5$–$2s2p^6$ transition dominates the spectrum. For the same reasons relative intensities of two spectral lines at $\lambda = 37.9$ nm and $\lambda = 48.9$ nm corresponding to $2s^2 2p^4$–$2s2p^5$ transitions in doubly charged Ne ions are comparable to $2s^2 2p^5$–$2s^2 2p^4 3l$ transitions in Ne II ions.

The spectra shown in Fig. 7 denoted as S1 and S2 were obtained for photoionized plasmas formed by the irradiation of Ne gas with SXR radiation pulses produced using the PALS laser system. The S1 spectrum corresponds to the case where unfiltered SXR radiation with the spectrum shown in Fig. 4(b) was used for direct irradiation of the Ne gas, injected in the vicinity of the laser plasma (Fig. 2). The S2 spectrum originates from the photoionized plasma driven by the focused SXR radiation filtered using two Al 750 nm thick foils limiting the radiation to the wavelength range $\lambda < 3$ nm (Fig. 3). In contrary to the spectrum from Fig. 6 both spectra contain intense K_α lines. Emission of K_α photons is connected to the inner shell ionization of neutral Ne atoms. The SXR photons with the energy exceeding the binding energy of K-shell electrons, E = 870.2 eV, dominate the spectrum of the ionizing radiation. A significant difference between S1 and S2 spectra concerns the long wavelength range. The S1 spectrum contains several overlapping lines corresponding to transitions in Ne III and Ne IV ions. These lines were not detected in case of the S2 spectrum. Apart from that no lines in EUV range corresponding to single charged ions were registered in both cases.

The mechanism leading to emission of Ne III and Ne IV spectral lines is connected with the initial inner shell ionization of the neutral atoms. Singly charged Ne ions with K-shell vacancies can relax emitting K_α photons or Auger electrons. Probability of the latter process is almost two orders of magnitude larger compared to the first one.[26] Additionally, a double Auger process is also possible.[27] In this way, doubly and triply charged ions are mostly produced. These ions can be then excited by the electron impact or photoexcitation. It would be quite worthy to note that the latter mechanism is strongly reduced in case where the Al filter was employed in the irradiation system as shown in Fig. 3. The lack of the spectral lines corresponding to the radiative transitions in Ne III and Ne IV ions in this case suggests that the dominant role in creation of the excited states plays photoexcitation.

The interferometric measurements allowed to determine the electron density distributions of the photoionized plasmas driven by the SXR pulses that were produced by using the PALS laser system. The maximum electron density calculated from the interferograms obtained for the delay times within the range of t = 0.5–2 ns, reaches the value of $2 \cdot 10^{18}\,\mathrm{cm}^{-3}$, corresponding to 10% of the atomic density under the atmospheric pressure. Similar value was measured for atomic density of the neutral gas injected into the vacuum chamber, utilizing an X-ray shadowgraphy.[28,29] This means that the average ionic charge was approximately 1. Taking into account that emission lines corresponding to doubly and triply charged ions were detected it can be concluded that the plasma also contains neutral atoms.

As discussed earlier in case of Ne plasmas, no interferogram was obtained for $t \approx 0$. For an earlier time t = −187 ps no fringe shift was detected, despite the laser plasma was well developed, as can be noticed from Fig. 8. This means that the electron density of the photoionized plasma at this time was below the detection limit. This limit can be estimated from Eq. (1). Assuming a minimum for detectable fringe shift $\delta = 0.2$, $\lambda = 8 \cdot 10^{-5}$ cm, and $l_p = 0.9$ cm we can obtain $n_e \approx 5 \cdot 10^{16}\,\mathrm{cm}^{-3}$. This value is the upper estimation of the electron density for the time t = −187 ps. In such a case, the ionization degree did not exceed 1%–2%. On the other hand, the interference pattern obtained for the Xe photoionized plasma at the time t = 33 ps, shown in Fig. 10, exhibits well shifted fringes. The maximum electron density value calculated for this case is only 2 times lower compared to the Ne plasmas formed afterwards. This demonstrates that the SXR emission at the time corresponding to the maximum

TABLE I. Summarized results of the comparative studies of photoionized plasmas created using three different irradiation systems: (−) sign denotes absence and (+) presence of the corresponding emission lines.

X-ray source/laser system	Maximum n_e	K-shell emission	L-shell emission			
			Ne I	Ne II	Ne III	Ne IV
EUV/SXR/NL 129	$<1.5{\cdot}10^{18}\,cm^{-3}$	−	+	+	+	−
SXR/PALS no collector	$>2{\cdot}10^{18}\,cm^{-3}$	+	−	−	+	+
SXR/PALS paraboloidal collector	Not measured	+	−	−	−	−

intensity of the laser pulse was sufficiently high for effective photoionization and formation of the photoionized plasma.

In case of interferometric measurements carried out for photoionized plasmas created using the NL129 laser system the detection limit was approximately $n_e \approx 1.5{\cdot}10^{18}\,cm^{-3}$. This limitation occurred due to approximately 20 times smaller plasma size along the diagnostic beam. It could be concluded that the electron density could reach in this case a similar value to that recorded when using the PALS laser system.

The most important differences observed between Ne plasmas produced using all the experimental arrangements are presented in Table I.

V. SUMMARY

In this paper, the results of investigations concerning low temperature photoionized plasmas created using two laser-produced plasma SXR/EUV sources of different parameters were presented. The photoionized plasmas were produced by irradiation of gases, injected into a vacuum chamber synchronously with the SXR/EUV pulses. The measurements of the emission spectra from the Ne photoionized plasmas in the SXR/EUV range were performed. The most intense spectral lines originated from singly charged ions, however, the spectral lines from doubly and triply charged ions, were also registered. Significant differences between the spectral compositions were observed. The differences mainly concern lines corresponding to K-shell and L-shell transitions, obtained using high and low energy irradiating systems, respectively. Various atomic processes dominating in the photoionized plasmas, that are responsible for the observed spectral differences, were discussed. The interference patterns were recorded for different instants of the photoionized plasma evolution employing the femtosecond laser system. Electron densities were calculated for Ne and Xe photoionized plasmas. This type of interferometry measurements concerning photoionized plasmas were performed for the first time. In all the previous works connected with laboratory astrophysics, as mentioned above and also other papers published recently,[30–32] the electron densities were estimated indirectly from initial atomic density and by fitting of calculated to the measured spectra.

ACKNOWLEDGMENTS

This work was supported by the National Science Centre, Poland, Grant Agreement No. UMO-2013/09/B/ST2/01625, European Commission's Seventh Framework Program (LASERLAB-EUROPE) Grant Agreement No. 284464 and by and the Czech Ministry of Education, Youth and Sport Grant Agreement No. LM2010014.

[1]J. E. Bailey, D. Cohen, G. Chandler, M. Cuneo, M. Foord, R. Heeter, D. Jobe, P. Lake, D. Liedahl, J. MacFarlane, T. Nash, D. Nielson, R. Smelser, and W. Stygar, J. Quant. Spectrosc. Radiat. Transfer **71**, 157 (2001).
[2]D. H. Cohen, J. J. MacFarlane, J. E. Bailey, and D. A. Liedahl, Rev. Sci. Instrum. **74**, 1962 (2003).
[3]S. Fujioka, H. Takabe, N. Yamamoto, D. Salzmann, F. Wang, H. Nishimura, Y. Li, Q. Dong, S. Wang, Y. Zhang, Y. Rhee, Y. Lee, J. Han, M. Tanabe, T. Fujiwara, Y. Nakabayashi, G. Zhao, J. Zhang, and K. Mima, Nature Phys. **5**, 821–825 (2009).
[4]H. G. Wei, J. R. Shi, G. Zhao, Y. Zhang, Q. L. Dong, Y. T. Li, S. J. Wang, J. Zhang, Z. T. Liang, J. Y. Zhang, T. S. Wen, W. H. Zhang, X. Hu, S. Y. Liu, Y. K. Ding, L. Zhang, Y. J. Tang, B. H. Zhang, Z. J. Zheng, H. Nishimura, S. Fujioka, F. L. Wang, and H. Takabe, Astrophys. J. **683**, 577–583 (2008).
[5]R. C. Mancini, J. E. Bailey, J. F. Hawley, T. Kallman, M. Witthoeft, S. J. Rose, and H. Takabe, Phys. Plasmas **16**, 041001 (2009).
[6]W. F. Huebner, J. J. Keady, and S. P. Lyon, Astrophys. Space Sci. **195**, 1–294 (1992).
[7]A. V. Pavlov, Surv. Geophys. **35**, 259–334 (2014).
[8]O. Dutuit, N. Carrasco, R. Thissen, V. Vuitton, C. Alcaraz, P. Pernot, N. Balucani, P. Casavecchia, A. Canosa, S. Le Picard, J.-C. Loison, Z. Herman, J. Zabka, D. Ascenzi, P. Tosi, P. Franceschi, S. D. Price, and P. Lavvas, Astrophys. J. **204**, 20 (2013).
[9]W. K. Peterson, T. N. Woods, J. M. Fontenla, P. G. Richards, P. C. Chamberlin, S. C. Solomon, W. K. Tobiska, and H. P. Warren, J. Geophys. Res. A **117**, A05320, doi:10.1029/2011JA017382 (2012).
[10]W. K. Peterson, D. A. Brain, D. L. Mitchell, S. M. Bailey, and P. C. Chamberlin, J. Geophys. Res. A **118**, 7338–7347 (2013).
[11]J. A. R. Samson and W. C. Stolte, J. Electron Spectrosc. Relat. Phenom. **123**, 265–276 (2002).
[12]J. W. Gallagher, C. E. Brion, J. A. R. Samson, and P. W. Langhoff, J. Phys. Chem. Ref. Data **17**, 9–153 (1988).
[13]Y. Itikawa, A. Ichimura, K. Onda, K. Sakimoto, K. Takayanagi, Y. Hatano, M. Hayashi, H. Nishimura, and S. Tsurubuchi, J. Phys. Chem. Ref. Data **18**, 23–42 (1989).
[14]W. S. Watson, J. Phys. B: At. Mol. Phys. **5**, 2292–2303 (1972).
[15]A. Bartnik, P. Wachulak, H. Fiedorowicz, T. Fok, R. Jarocki, and M. Szczurek, Phys. Plasmas **20**, 113302 (2013).
[16]A. Bartnik, R. Fedosejevs, P. Wachulak, H. Fiedorowicz, C. Serbanescu, E. G. Saiz, D. Riley, S. Toleikis, and D. Neely, Laser Particle Beams **31**, 195–201 (2013).
[17]A. Bartnik, P. Wachulak, H. Fiedorowicz, R. Jarocki, J. Kostecki, and M. Szczurek, Radiat. Phys. Chem. **93**, 9–14 (2013).
[18]A. Bartnik, H. Fiedorowicz, and P. Wachulak, Phys. Plasmas **21**, 073303 (2014).
[19]A. Bartnik, P. Wachulak, H. Fiedorowicz, T. Fok, R. Jarocki, and M. Szczurek, Phys. Scr. **T161**, 014061 (2014).
[20]A. Bartnik, H. Fiedorowicz, R. Rakowski, M. Szczurek, F. Bijkerk, R. Bruijn, and H. Fledderus, "Soft x-ray emission from a double stream gas puff target irradiated by a nanosecond laser pulse," in *ECLIM 2000: 26th European Conference on Laser Interaction with Matter*, edited by M. Kálal, K. Rohlena, and M. Šinor [Proc. SPIE, **4424**, 406–409 (2001)].
[21]H. Fiedorowicz, A. Bartnik, H. Daido, Il. Woo Choi, M. Suzuki, and S. Yamagami, Opt. Commun. **184**, 161–167 (2000).
[22]M. L. Schattenburg, E. H. Anderson, and H. I. Smith, Phys. Scr. **41**, 13–20 (1990).

[23]T. Pisarczyk, S. Yu. Gus'kov, Z. Kalinowska, J. Badziak, D. Batani, L. Antonelli, G. Folpini, Y. Maheut, F. Baffigi, S. Borodziuk, T. Chodukowski, G. Cristoforetti, N. N. Demchenko, L. A. Gizzi, A. Kasperczuk, P. Koester, E. Krousky, L. Labate, P. Parys, M. Pfeifer, O. Renner, M. Smid, M. Rosinski, J. Skala, R. Dudzak, J. Ullschmied, and P. Pisarczyk, Phys. Plasmas **21**, 012708 (2014).
[24]T. Pisarczyk, S. Yu. Gus'kov, O. Renner, N. N. Demchenko, Z. Kalinowska, T. Chodukowski, M. Rosinski, P. Parys, M. Smid, J. Dostal, J. Badziak, D. Batani, L. Volpe, E. Krousky, R. Dudzak, J. Ullschmied, H. Turcicova, J. Hrebicek, T. Medrik, M. Pfeifer, J. Skala, A. Zaras-Szydlowska, L. Antonelli, Y. Maheut, S. Borodziuk, A. Kasperczuk, and P. Pisarczyk, "Pre-plasma effect on laser beam energy transfer to a dense target under conditions relevant to shock ignition," Laser Part. Beams (published online 2015).
[25]A. Kasperczuk and T. Pisarczyk, Opt. Appl. **XXXI**(3), 571–597 (2001).
[26]M. O. Krause, J. Phys. Chem. Ref. Data **8**, 307 (1979).
[27]A. G. Kochur, V. L. Sukhorukov, and V. F. Demekhin, J. Electron Spectrosc. Relat. Phenom. **137–140**, 325–328 (2004).
[28]A. Bartnik, V. M. Dyakin, I. YU. Skobelev, A. Ya. Faenov, H. Fiedorowicz, and M. Szczurek, Quan. Electr. **27**, 68–71 (1997).
[29]A. Bartnik, W. Lisowski, J. Sobczak, P. Wachulak, B. Budner, B. Korczyc, and H. Fiedorowicz, Appl. Phys. A **109**, 39–43 (2012).
[30]G. A. Rochau, J. E. Bailey, R. E. Falcon, G. P. Loisel, T. Nagayama, R. C. Mancini, I. Hall, D. E. Winget, M. H. Montgomery, and D. A. Liedahl, Phys. Plasmas **21**, 056308 (2014).
[31]I. M. Hall, T. Durmaz, R. C. Mancini, J. E. Bailey, G. A. Rochau, I. E. Golovkin, and J. J. MacFarlane, Phys. Plasmas **21**, 031203 (2014).
[32]G. Y. Liang, F. Li, F. L. Wang, Y. Wu, J. Y. Zhong, and G. Zhao, Astrophys. J. **783**, 124 (2014).